# Experimental Measurement and Thermodynamic Modeling of the Mixed CH4 + C3H8 Clathrate Hydrate Equilibria in Silica Gel Pores: Effects of Pore Size and Salinity

**ARTICLE** *in* LANGMUIR · JUNE 2010

Impact Factor: 4.46 · DOI: 10.1021/la100466s · Source: PubMed



**2 AUTHORS**, INCLUDING:

Yongwon Seo
Ulsan National Institute of Science and Tech…

**55** PUBLICATIONS **1,062** CITATIONS

SEE PROFILE

Langmuir
Article
pubs.acs.org/Langmuir


# Experimental Measurement and Thermodynamic Modeling of the Mixed $CH_4 + C_3H_8$ Clathrate Hydrate Equilibria in Silica Gel Pores: Effects of Pore Size and Salinity

Seungmin Lee and Yongwon Seo*

*Department of Chemical Engineering, Changwon National University, 9 Sarim-dong, Changwon, Gyeongnam 641-773, Republic of Korea*

*Received February 1, 2010. Revised Manuscript Received March 31, 2010*

We measured hydrate phase equilibria for the ternary $CH_4$ (90%) + $C_3H_8$ (10%) + water mixtures in silica gel pores with nominal diameters of 6.0, 15.0, 30.0, and 100.0 nm and for the quaternary $CH_4$ (90%) + $C_3H_8$ (10%) + NaCl + water mixtures of two different NaCl concentrations (3 and 10 wt %) in silica gel pores with nominal diameters of 6.0, 15.0, and 30.0 nm. The $CH_4$ (90%) + $C_3H_8$ (10%) hydrate−water interfacial tension ($\sigma_{HW}$) of $42 \pm 3$ mJ/m$^2$ was obtained through the Gibbs−Thomson equation for dissociation within cylindrical pores. With this value, the experimental results were in good agreement with the calculated ones based on the van der Waals and Platteeuw model. A correction term for the capillary effect and a Pitzer model for electrolyte solutions were adopted to calculate the activity of water in the aqueous electrolyte solutions within silica gel pores. At a specified temperature, three-phase H−$L_W$−V equilibrium curves of pore hydrates were shifted to higher-pressure regions depending on pore sizes and NaCl concentrations. From the cage-dependent $^{13}$C NMR chemical shifts of enclathrated guest molecules, the mixed $CH_4$ (90%) + $C_3H_8$ (10%) gas hydrate was confirmed to be structure II.

## Introduction

Gas hydrates are nonstoichiometric crystalline compounds formed when "guest" molecules of a suitable size and shape are incorporated into the well-defined cages in the "host" lattice made up of hydrogen-bonded water molecules. These compounds exist in three distinct structures, structure I (sI), structure II (sII), and structure H (sH), which contain differently sized and shaped cages.[1] Large masses of natural gas hydrates exist in permafrost regions or beneath deep oceans, where they are commonly found in sand or clay-type sediments. These naturally occurring gas hydrates in the earth containing mostly $CH_4$ are regarded as future energy resources.[1] Even though the equilibrium pressure for hydrate dissociation and the thermodynamic properties in large pores of coarse-grained sand sediment are nearly identical to those in the pure bulk water phase, for the exploitation of the natural gas hydrate in the sediments of fine-grained sand or clay it is very important to consider the complicated effects of both pores and electrolytes on the formation of mixed-gas hydrates. However, to the best of our knowledge, very little research on mixed-gas hydrates containing electrolytes in porous media appears in the literature, even though quite a few studies separately covering either porous media or electrolyte effects are found in various sources. Handa and Stupin[2] first studied the pore effect on the equilibrium pressures of $CH_4$ and $C_3H_8$ hydrates. Uchida et al.,[3,4] Smith et al.,[5] Zhang et al.,[6] Seo et al.,[7,8] Anderson et al.,[9,10] and Kang et al.[11] reported pore equilibrium pressure−temperature data for gas hydrates of a single guest such as $CH_4$, $CO_2$, $C_2H_6$, or $C_3H_8$. Østergaard et al.[12] presented experimental $CH_4$ hydrate dissociation data for methanol solutions in confined pores. Seo and Lee[13] examined the phase equilibria of $CH_4$ and $CO_2$ hydrates in silica gel pores filled with NaCl solution.

The complex phase behavior of the mixed-gas hydrate systems containing both multiguest components and electrolytes in porous media must be investigated a priori to provide basic and exact information on the exploration and exploitation of natural gas hydrates. Therefore, we newly attempt to provide key information on the electrolyte effects on the phase equilibrium behavior of mixed-gas hydrates, particularly in porous media. First, the hydrate phase equilibria for the ternary $CH_4$ (90%) + $C_3H_8$ (10%) + water mixtures in silica gel pores with nominal diameters of 6.0, 15.0, 30.0, and 100.0 nm were measured to check the pore-size effects on the mixed-gas hydrate equilibrium. Second, the hydrate phase equilibria for the quaternary $CH_4$ (90%) + $C_3H_8$ (10%) + NaCl + water mixtures of 3 wt % NaCl concentration in silica gel pores with nominal diameters of 6.0, 15.0, and 30.0 nm were determined to examine the pore effects on mixed-gas hydrate formation containing electrolyte. Third, the hydrate phase equilibria for the quaternary $CH_4$ (90%) + $C_3H_8$ (10%) + NaCl + water mixtures were measured in nominal 30.0 nm silica gel pores at two different NaCl concentrations of 3 and 10 wt % to investigate the combined effect of pores and electrolytes occurring in the surroundings of the deep ocean sediments. All of these

*To whom correspondence should be addressed. Tel: 82-55-213-3757. Fax: 82-55-283-6465. E-mail: yseo@changwon.ac.kr.

(1) Sloan, E. D.; Koh, C. A. *Clathrate Hydrates of Natural Gases*, 3rd ed.; CRC Press: Boca Raton, FL, 2008.
(2) Handa, Y. P.; Stupin, D. *J. Phys. Chem.* **1992**, *96*, 8599.
(3) Uchida, T.; Ebinuma, T.; Ishizaki, T. *J. Phys. Chem. B* **1999**, *103*, 3659.
(4) Uchida, T.; Ebinuma, T.; Takeya, S.; Nagao, J.; Narita, H. *J. Phys. Chem. B* **2002**, *106*, 820.
(5) Smith, D. H.; Wilder, J. W.; Seshadri, K. *AIChE J.* **2002**, *48*, 393.
(6) Zhang, W.; Wilder, J. W.; Smith, D. H. *AIChE J.* **2002**, *48*, 2324.
(7) Seo, Y.; Lee, H.; Uchida, T. *Langmuir* **2002**, *18*, 9164.
(8) Seo, Y.; Lee, S.; Cha, I.; Lee, J. D.; Lee, H. *J. Phys. Chem. B* **2009**, *113*, 5487.
(9) Anderson, R.; Llamedo, M.; Tohidi, B.; Burgass, R. W. *J. Phys. Chem. B* **2003**, *107*, 3500.
(10) Anderson, R.; Llamedo, M.; Tohidi, B.; Burgass, R. W. *J. Phys. Chem. B* **2003**, *107*, 3507.
(11) Kang, S.-P.; Lee, J.-W.; Ryu, H.-J. *Fluid Phase Equilib.* **2008**, *274*, 68.
(12) Østergaard, K. K.; Anderson, R.; Llamedo, M.; Tohidi, B. *Terra Nova* **2002**, *14*, 307.
(13) Seo, Y.; Lee, H. *J. Phys. Chem. B* **2003**, *107*, 889.

**Table 1. Physical Properties of Silica Gel Samples[a,b]**

| sample | 12.9 (6.0) nm | 22.6 (15.0) nm | 56.6 (30.0) nm | 165.2 (100.0) nm |
|---|---|---|---|---|
| mean particle diameter ($\mu$m) | 33−74 | 33−74 | 40−75 | 40−75 |
| mean pore diameter (nm) | 6.8 (6.0) | 14.6 (15.0) | 30.5 (30.0) | 94.5 (100.0) |
| maximum pore diameter (nm) | 12.9 | 22.6 | 56.6 | 165.2 |
| pore volume ($cm^3/g$) | 0.84 (0.75) | 1.13 (1.15) | 0.84 | 0.83 |
| surface area ($m^2/g$) | 497 (480) | 308 (300) | 111 (100) | 42.4 (50) |

[a] Values in the parentheses are vendor data. [b] 12.9 (6.0) nm: maximum pore diameter (nominal pore diameter).

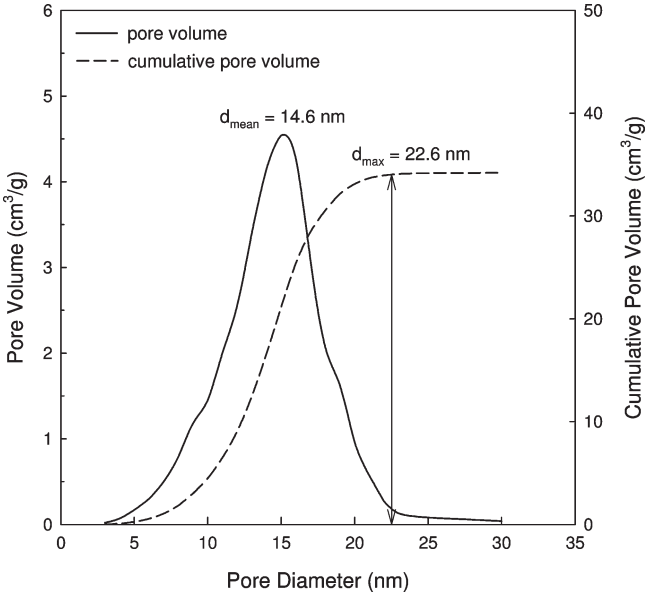


**Figure 1.** Pore-size distribution and cumulative pore-size distribution of a nominal 15.0 nm silica gel.

measured data were compared with calculated values based on the van der Waals and Platteeuw model incorporated with two additional terms considering pores and electrolytes. Furthermore, the $^{13}C$ NMR spectra were examined to identify and confirm the structure of the mixed $CH_4$ (90%) + $C_3H_8$ (10%) gas hydrate.

## Experimental Section

**Materials.** The mixed $CH_4$ (90%) + $C_3H_8$ (10%) gas used for the present study was supplied by Gyeongdong Industrial Gas Co. (Korea). Silica gels with nominal pore diameters of 6.0 and 15.0 nm were purchased from Aldrich. Silica gels with nominal pore diameters of 30.0 and 100.0 nm were purchased from Silicycle Co. (Canada). All materials were used without further treatment. The properties of silica gels having four different pore diameters were measured by ASAP 2420 and Autopore IV 9520 (Micromeritics) and are listed in Table 1. Figure 1 shows the pore-size distribution and cumulative pore-size distribution of a nominal 15.0 nm silica gel sample. As shown in Figure 1, the maximum pore diameter of each silica gel sample was determined to be the pore diameter corresponding to a 99.5% value of each final cumulative pore volume. Hereafter, for clarity, the silica gel sample will be expressed as the maximum diameter (nominal diameter) in the text, for example, 12.9 (6.0) nm.

**Apparatus and Procedure.** In the present study, water or electrolyte solutions should exist only within pores of silica gels to examine the pore effect on the hydrate phase equilibria. To prepare the pore-saturated silica gels, the silica gels were first dried at 393 K for 24 h before water sorption. Some amount of dried silica gel powder was placed in a bottle, and an amount of water or electrolyte solution identical to the pore volume of the silica gel was added to the powder. After mixing, the bottle was sealed with a cap to prevent water evaporation. Then, the bottle was vibrated with ultrasonic waves at 293.15 K for 24 h to fill the pores completely with water or electrolyte solutions.

The experimental apparatus for hydrate phase equilibria was specially designed to measure the hydrate dissociation pressures and temperatures accurately. The equilibrium cell was made of 316 stainless steel and had an internal volume of about 150 $cm^3$. The experiment for hydrate phase-equilibrium measurements began by charging the equilibrium cell with about 80 $cm^3$ of silica gels containing pore water or electrolyte solutions. After the equilibrium cell was pressurized to the desired pressure with mixed $CH_4$ (90%) + $C_3H_8$ (10%) gas, the whole main system was slowly cooled to a temperature lower than the expected equilibrium temperature. When pressure depression due to hydrate formation reached a steady-state condition, the cell temperature was increased in 0.3 K steps over 2 h of equilibration time for samples of all pore sizes used in this study, which was confirmed to be sufficient by checking pressure ($P$) versus time ($t$) curves for each step.

The equilibrium pressure and temperature of the three phases (hydrate (H) − water-rich liquid ($L_W$) − vapor (V)) in the silica gel pores should be determined by considering the pore-size distribution of the silica gels. For the gas hydrates of a single guest, the dissociation equilibrium point in silica gel pores was chosen as the inflection point of the pressure ($P$) versus temperature ($T$) heating curve, which corresponds to the extremum point of the $dP/dT$ versus $T$ heating curve. The inflection point of the $P$ versus $T$ heating curve corresponds to the equilibrium dissociation point in the pores of the mean diameter ($d_{mean}$) of the silica gels used.[8,9] However, for the mixed-gas hydrates or hydrates made from electrolyte solutions, the inflection point of the $P$ versus $T$ heating curve does not correspond to the initial gas composition or electrolyte concentration. For the mixed $CH_4$ (90%) + $C_3H_8$ (10%) gas hydrate, the $CH_4$ composition of the gas phase in the H−$L_W$−V equilibrium point determined from a mean diameter consideration will be higher than the initial 90% because $C_3H_8$, whose hydrate equilibrium condition is remarkably milder than $CH_4$, is enriched in the hydrate phase. In addition, gas hydrate formed in pores with a certain mean diameter will be in equilibrium with an electrolyte solution of higher concentration than the initial concentration because hydrate lattices exclude electrolytes, resulting in an increase in the electrolyte concentration of the liquid water phase in the H−$L_W$−V equilibrium. Therefore, for systems with mixed-gas hydrates or with an electrolyte present, the gas-phase composition of the mixed-gas hydrates or the electrolyte concentration in the liquid water phase becomes equal to the initial conditions only at the point of final pore hydrate dissociation (i.e., maximum pore diameter ($d_{max}$)).

Figure 2 shows one example of the $P$ versus $T$ heating curve for the $CH_4$ (90%) + $C_3H_8$ (10%) + NaCl (3 wt %) + water mixtures in 22.6 (15.0) nm silica gel pores. Unlike the bulk hydrate, a gradual change in slope around the final hydrate dissociation point was observed because of the pore-size distribution. To account for the pore-size distribution, initial gas composition, and initial electrolyte concentration accurately, the hydrate dissociation equilibrium point in silica pores was chosen in the present study as the final pore hydrate dissociation point that corresponds to the hydrate dissociation at $d_{max}$.

To identify the crystal structure of the mixed $CH_4$ (90%) + $C_3H_8$ (10%) gas hydrate, a Bruker 400 MHz solid-state NMR spectrometer that belongs to the Korea Basic Science Institute (KBSI) was used in this study. The NMR spectra were recorded at

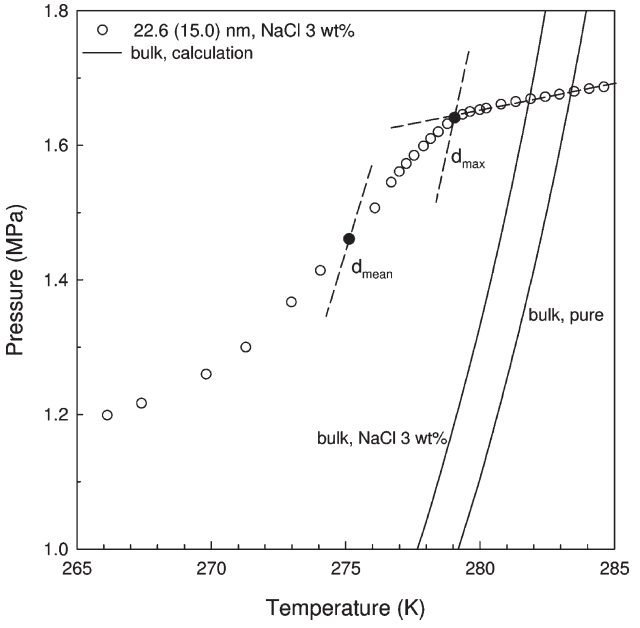


**Figure 2.** $P$ versus $T$ heating curve for the $CH_4$ (90%) + $C_3H_8$ (10%) + NaCl (3 wt %) + water mixtures in 22.6 (15.0) nm silica gel pores.

243 K by placing the hydrate samples within a 4 mm o.d. Zr rotor that was loaded into the variable temperature (VT) probe. All $^{13}C$ NMR spectra were recorded at a Larmor frequency of 100.6 MHz with magic angle spinning (MAS) at about 2−4 kHz. A pulse length of 2 $\mu$s and a pulse repetition delay of 10 s under proton decoupling were employed when the radio frequency field strengths of 50 kHz corresponding to 5 $\mu$s 90° pulses were used. The downfield carbon resonance peak of adamantane, assigned a chemical shift of 38.3 ppm at 300 K, was used as an external chemical shift reference. A more detailed description of the experimental apparatus and procedure was given in previous papers.[7,8,13]

**Thermodynamic Model.** The equilibrium criteria of the hydrate-forming mixture are based on the equality of fugacities of specified component $i$ in all phases that coexist simultaneously

$$\hat{f}_i^{\mathrm{H}} = \hat{f}_i^{\mathrm{L}} = \hat{f}_i^{\mathrm{V}} (= f_{\mathrm{w}}^{\mathrm{I}}) \tag{1}$$

where H stands for the hydrate phase, L stands for the water-rich liquid phase, V stands for the vapor phase, and I stands for the ice phase. It can be reasonably assumed that electrolytes are completely excluded from the hydrate lattice and remain only in the liquid phase.

The chemical potential difference between the empty hydrate and filled hydrate phases, $\Delta\mu_{\mathrm{w}}^{\mathrm{MT-H}} (= \mu_{\mathrm{w}}^{\mathrm{MT}} - \mu_{\mathrm{w}}^{\mathrm{H}})$, is generally derived from statistical mechanics in the van der Waals and Platteeuw model[14]

$$\Delta\mu_{\mathrm{w}}^{\mathrm{MT-H}} = \mu_{\mathrm{w}}^{\mathrm{MT}} - \mu_{\mathrm{w}}^{\mathrm{H}} = -RT\sum_m \nu_m \ln\left(1 - \sum_j \theta_{mj}\right) \tag{2}$$

where $\mu_{\mathrm{w}}^{\mathrm{MT}}$ is the chemical potential of water in the hypothetical empty hydrate lattice, $\nu_m$ is the number of cavities of type $m$ per water molecule in the hydrate phase, and $\theta_{mj}$ is the fraction of cavities of type $m$ occupied by molecules of component $j$. This fractional occupancy is determined by a Langmuir-type expression

$$\theta_{mj} = \frac{C_{mj}\hat{f}_j^{\mathrm{V}}}{1 + \sum_k C_{mk}\hat{f}_k^{\mathrm{V}}} \tag{3}$$

where $C_{mj}$ is the Langmuir constant of component $j$ on the cavity of type $m$ and $\hat{f}_j^{\mathrm{V}}$ is the fugacity of component $j$ in the vapor phase with which the hydrate phase is in equilibrium.

The Langmuir constant, $C_{mj}$, is

$$C_{mj} = \frac{4\pi}{kT}\int_0^\infty \exp\left[\frac{-\omega(r)}{kT}\right] r^2\, \mathrm{d}r \tag{4}$$

where $k$ is the Boltzmann constant, $r$ is the radial distance from the cavity center, and $\omega(r)$ is the spherical-core potential. In the present study, the Kihara potential with the spherical core is used for the cavity potential function.

Holder et al.[15] suggested a method to simplify the chemical potential difference between the empty hydrate and the reference state as follows

$$\frac{\Delta\mu_{\mathrm{w}}^{\mathrm{MT-L}}}{RT} = \frac{\Delta\mu_{\mathrm{w}}^{0}}{RT} - \int_{T_0}^{T} \frac{\Delta h_{\mathrm{w}}^{\mathrm{MT-I}} + \Delta h_{\mathrm{w}}^{\mathrm{fus}}}{RT^2}\,\mathrm{d}T + \int_0^P \frac{\Delta v_{\mathrm{w}}^{\mathrm{MT-I}} + \Delta v_{\mathrm{w}}^{\mathrm{fus}}}{RT}\,\mathrm{d}P - \ln a_{\mathrm{w}} \tag{5}$$

where $T_0$ is 273.15 K, the normal melting point of water, $\Delta\mu_{\mathrm{w}}^{0}$ is the chemical potential difference between the empty hydrate and water at $T_0$ and zero absolute pressure, $\Delta h_{\mathrm{w}}^{\mathrm{MT-}I}$ and $\Delta v_{\mathrm{w}}^{\mathrm{MT-}I}$ are the molar differences in enthalpy and volume between the empty hydrate and ice, respectively, and $\Delta h_{\mathrm{w}}^{\mathrm{fus}}$ and $\Delta v_{\mathrm{w}}^{\mathrm{fus}}$ are the molar differences in enthalpy and volume between ice and liquid water, respectively. $a_{\mathrm{w}}$ denotes the activity of water calculated from an equation of state and is equivalent to the product of the activity coefficient of water, $\gamma_{\mathrm{w}}$, and the mole fraction of water, $x_{\mathrm{w}}$.

If the equilibrium temperature is above the ice point, then the fugacity of water in the filled hydrate lattice, $\hat{f}_{\mathrm{w}}^{\mathrm{H}}$, is calculated by the following expression

$$\hat{f}_{\mathrm{w}}^{\mathrm{H}} = f_{\mathrm{w}}^{\mathrm{L}} \exp\left(\frac{\Delta\mu_{\mathrm{w}}^{\mathrm{MT-L}}}{RT} - \frac{\Delta\mu_{\mathrm{w}}^{\mathrm{MT-H}}}{RT}\right) \tag{6}$$

where $\Delta\mu_{\mathrm{w}}^{\mathrm{MT-L}} = \mu_{\mathrm{w}}^{\mathrm{MT}} - \mu_{\mathrm{w}}^{\mathrm{L}}$.

The fugacity coefficient of water, $\varphi_{\mathrm{w}}$, in the aqueous electrolyte liquid phase is given by the model of Aasberg-Petersen et al.[16]

$$\ln \varphi_{\mathrm{w}} = \ln \varphi_{\mathrm{w}}^{\mathrm{EOS}} + \ln \gamma_{\mathrm{w}}^{\mathrm{EL}} \tag{7}$$

where $\gamma_{\mathrm{w}}^{\mathrm{EL}}$ stands for the activity coefficient of water in an electrolyte solution.

The first term for the normal contribution can be calculated from the Soave−Redlich−Kwong (SRK) equation of state (EOS), and the second term for the electrolyte contribution can be calculated from the Pitzer model[17]

$$\gamma_{\mathrm{w}}^{\mathrm{EL}} = \frac{a_{\mathrm{w}}^{\mathrm{EL}}}{x_{\mathrm{w}}} \tag{8}$$

$$\ln a_{\mathrm{w}}^{\mathrm{EL}} = -\frac{M_{\mathrm{w}}\nu m}{1000}\phi \tag{9}$$

where $a_{\mathrm{w}}^{\mathrm{EL}}$ stands for the activity of water in an electrolyte solution, $M_{\mathrm{w}}$ stands for the molecular weight of water, $m$ stands for the molality of the electrolyte, $\nu$ stands for the number of ions

(14) van der Waals, J. H.; Platteeuw, J. C. *Adv. Chem. Phys.* **1959**, *2*, 1.

(15) Holder, G. D.; Corbin, G.; Papadopoulos, K. D. *Ind. Eng. Chem. Fundam.* **1980**, *19*, 282.

(16) Aasberg-Petersen, K.; Stenby, E.; Fredenslund, A. *Ind. Eng. Chem. Res.* **1991**, *30*, 2180.

(17) Pitzer, K. S. *J. Phys. Chem.* **1973**, *77*, 268.

the electrolytes dissociates into, and $\phi$ stands for the osmotic coefficient.

The decrease in water activity in silica gel pores filled with electrolyte solution can be expressed as[7,18]

$$\ln a_w = \ln a_w^{EL} - \frac{FV_L \cos\theta\, \sigma_{HW}}{rRT} \quad (10)$$

where $F$ is the shape factor, a function of the curvature of the hydrate−liquid interface, $V_L$ is the molar volume of pure water, $\theta$ is the wetting angle between pure water and hydrate phases, $\sigma_{HW}$ is the interfacial tension between hydrate and liquid water phases, and $r$ is the pore radius. In the present study, $F = 1$ was used for hydrate dissociation in narrow pores. Combining and solving the above equations determines the values of the H−$L_W$−V equilibrium pressure and temperature for the pore radius and electrolyte concentration.

The fugacities of supercooled water and all components in the vapor phase, $f_w^L$ and $\hat{f}_j^V$, were calculated using SRK-EOS incorporated with the modified Huron−Vidal second-order mixing rule.[19] The optimized Kihara potential parameters used in this study and more details of the model description were given in our previous papers.[7,8,13]

## Results and Discussion

To understand the pore effect on the hydrate formation/dissociation and thermodynamic modeling of the pore equilibrium of the mixed $CH_4 + C_3H_8$ gas hydrates, the operative interface of the hydrate and liquid water phases is crucial. However, no information on the mixed $CH_4 + C_3H_8$ gas hydrate−water interfacial tension ($\sigma_{HW}$) has been reported in the literature. To relate the dissociation temperature depression (from bulk conditions) with the pore size of silica gels at a given pressure, the Gibbs−Thomson equation was used in this study. According to this relationship, the temperature depression of hydrate dissociation in a cylindrical pore, $\Delta T_{m,pore}$, relative to the bulk dissociation temperature, $T_{m,bulk}$, is defined as[9,20]

$$\frac{\Delta T_{m,pore}}{T_{m,bulk}} = -\left(\frac{\sigma_{HW}\cos\theta}{\rho_h \Delta H_{h,d}\, r}\right) \quad (11)$$

where $\Delta T_{m,pore}$ is the difference between the pore ($T_{m,pore}$) and bulk dissociation temperature, $T_{m,bulk}$, at a specified pressure, $\rho_h$ is the hydrate density, $\Delta H_{h,d}$ is the hydrate dissociation enthalpy, and $r$ is the pore radius.

As shown in Figure 3, the interfacial tension between the hydrate and water phase can be estimated from the slope of the plot of the reciprocal pore diameter ($^1/_d$) versus $\Delta T_{m,pore}/T_{m,bulk}$ for hydrate dissociation in silica gel pores. For the mixed $CH_4 + C_3H_8$ gas hydrate, a value of $\Delta H = 79.2$ kJ/mol was given using the Clausius−Clapeyron equation with pressure−temperature data of three-phase H−$L_W$−V equilibrium.[21] From the thermodynamic modeling for the mixed $CH_4$ (90%) + $C_3H_8$ (10%) gas hydrate, the hydrate density can be assumed to be 941 kg/m$^3$. Applying all these values to eq 11, an average value for the mixed $CH_4$ (90%) + $C_3H_8$ (10%) gas hydrate−water interfacial tension of 42 ± 3 mJ/m$^2$ was obtained from the slope of the data in Figure 3. To the best of our knowledge, the value for the mixed $CH_4 + C_3H_8$ gas hydrate−water interfacial tension was obtained for the first time in this work. This value is larger than that of the

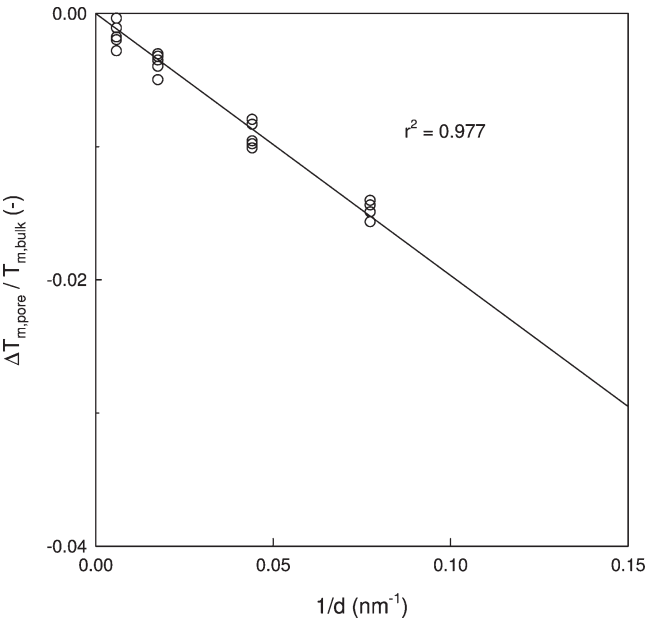


**Figure 3.** Plot of the reciprocal pore diameter ($^1/_d$) vs $\Delta T_{m,pore}/T_{m,bulk}$ for the mixed $CH_4$ (90%) + $C_3H_8$ (10%) hydrates in silica gel pores.

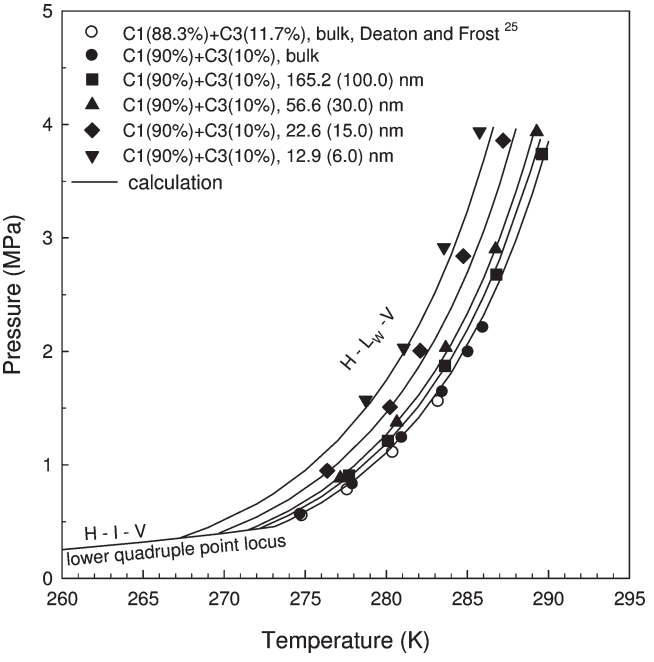


**Figure 4.** Hydrate-phase equilibria of the ternary $CH_4$ (90%) + $C_3H_8$ (10%) + water mixtures in silica gel pores.

$CH_4$ hydrate−water interfacial tension, 32 ± 1 mJ/m$^2$, and slightly smaller than that of the $C_3H_8$ hydrate−water interfacial tension, 45 ± 1 mJ/m.[2,8,10]

Three-phase H−$L_W$−V equilibria for the ternary $CH_4$ (90%) + $C_3H_8$ (10%) + water mixtures in 12.9 (6.0), 22.6 (15.0), 56.6 (30.0), and 165.2 (100.0) nm silica gel pores were measured and presented along with model calculations in Figure 4 and Table 2. As is the case of the binary gas + water mixtures in silica gel pores, the presence of geometrical constraints caused the H−$L_W$−V curves to be shifted to the inhibition region represented by lower temperature and higher pressure conditions than those in the bulk state. Three-phase H−$L_W$−V equilibria for the

(18) Llamedo, M.; Anderson, R.; Tohidi, B. *Am. Miner.* **2004**, *89*, 1264.
(19) Dahl, S.; Fredenslund, A.; Rasmussen, P. *Ind. Eng. Chem. Res.* **1991**, *30*, 1936.
(20) Clennell, M. B.; Hovland, M.; Booth, J. S.; Henry, P.; Winters, W. J. *J. Geophys. Res.* **1999**, *104*, 22985.
(21) Sloan, E. D.; Fleyfel, F. *Fluid Phase Equilib.* **1992**, *76*, 123.

**Table 2. Hydrate Phase Equilibrium Data for the $CH_4 + C_3H_8$ + Water Mixtures in Silica Gel Pores**

| 12.9 (6.0) nm | | 22.6 (15.9) nm | | 56.6 (30.0) nm | | 165.2 (100.0) nm | | bulk | |
|---|---|---|---|---|---|---|---|---|---|
| $T$ (K) | $P$ (MPa) | $T$ (K) | $P$ (MPa) | $T$ (K) | $P$ (MPa) | $T$ (K) | $P$ (MPa) | $T$ (K) | $P$ (MPa) |
| 278.72 | 1.573 | 276.36 | 0.949 | 277.16 | 0.884 | 277.71 | 0.906 | 274.69 | 0.564 |
| 281.07 | 2.03 | 280.23 | 1.51 | 280.65 | 1.376 | 280.09 | 1.211 | 277.92 | 0.83 |
| 283.56 | 2.917 | 282.1 | 2.006 | 283.67 | 2.033 | 283.62 | 1.872 | 280.96 | 1.239 |
| 285.75 | 3.936 | 284.76 | 2.839 | 286.73 | 2.901 | 286.79 | 2.677 | 283.46 | 1.643 |
| | | 287.21 | 3.858 | 289.28 | 3.935 | 289.6 | 3.739 | 285.05 | 1.994 |
| | | | | | | | | 285.95 | 2.21 |

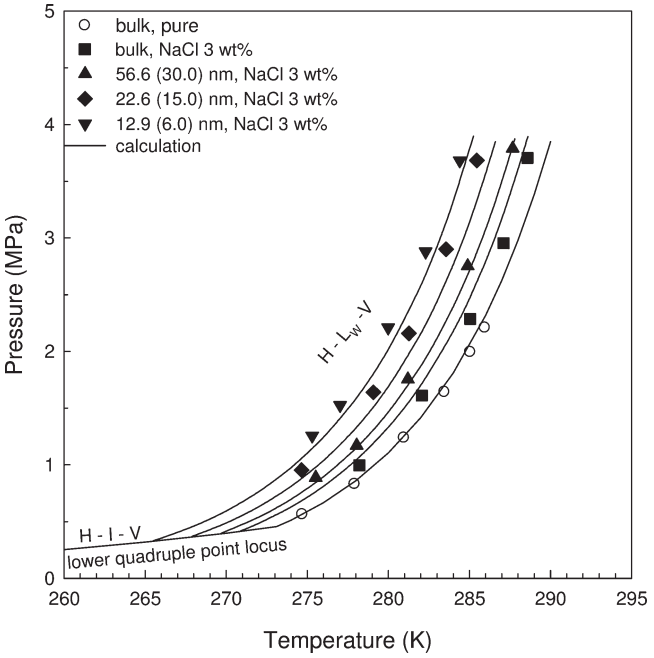


**Figure 5.** Hydrate phase equilibria of the quaternary $CH_4$ (90%) + $C_3H_8$ (10%) + NaCl (3 wt %) + water mixtures in silica gel pores.

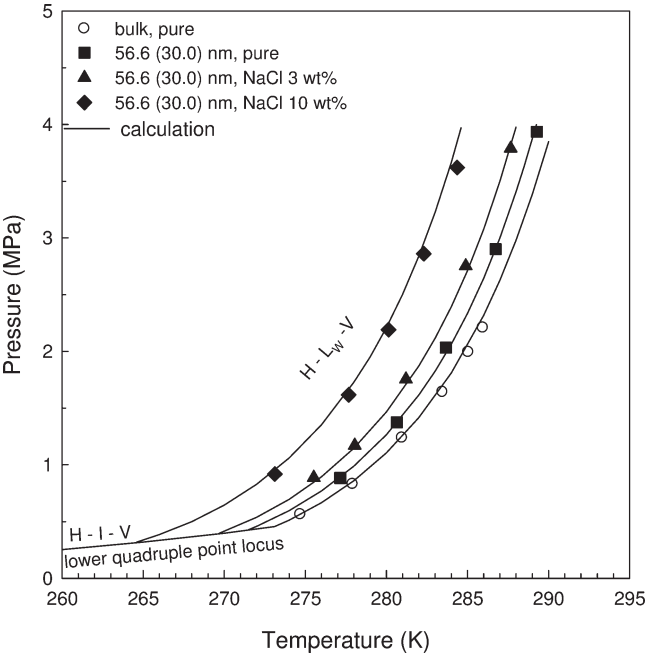


**Figure 6.** Hydrate phase equilibria of the quaternary $CH_4$ (90%) + $C_3H_8$ (10%) + NaCl + water mixtures in 56.6 (30.0) nm silica gel pores.

**Table 3. Hydrate Phase Equilibrium Data for the $CH_4 + C_3H_8$ + NaCl (3 wt %) + Water Mixtures in Silica Gel Pores**

| 12.9 (6.0) nm | | 22.6 (15.9) nm | | 56.6 (30.0) nm | | bulk | |
|---|---|---|---|---|---|---|---|
| $T$ (K) | $P$ (MPa) | $T$ (K) | $P$ (MPa) | $T$ (K) | $P$ (MPa) | $T$ (K) | $P$ (MPa) |
| 275.3 | 1.257 | 274.65 | 0.954 | 275.52 | 0.888 | 278.21 | 0.998 |
| 277.03 | 1.526 | 279.07 | 1.64 | 278.05 | 1.171 | 282.06 | 1.611 |
| 279.99 | 2.211 | 281.27 | 2.16 | 281.21 | 1.755 | 285.03 | 2.287 |
| 282.3 | 2.88 | 283.56 | 2.901 | 284.9 | 2.753 | 287.1 | 2.953 |
| 284.4 | 3.683 | 285.45 | 3.684 | 287.67 | 3.789 | 288.58 | 3.705 |

**Table 4. Hydrate Phase Equilibrium Data for the $CH_4 + C_3H_8$ + NaCl + Water Mixtures in 56.6 (30.0) nm Silica Gel Pores**

| pure | | 3 wt % | | 10 wt % | |
|---|---|---|---|---|---|
| $T$ (K) | $P$ (MPa) | $T$ (K) | $P$ (MPa) | $T$ (K) | $P$ (MPa) |
| 277.16 | 0.884 | 275.52 | 0.888 | 273.12 | 0.919 |
| 280.65 | 1.376 | 278.05 | 1.171 | 277.68 | 1.617 |
| 283.67 | 2.033 | 281.21 | 1.755 | 280.13 | 2.191 |
| 286.73 | 2.901 | 284.9 | 2.753 | 282.31 | 2.861 |
| 289.28 | 3.935 | 287.67 | 3.789 | 284.37 | 3.62 |

quaternary $CH_4$ (90%) + $C_3H_8$ (10%) + NaCl + water mixtures in 12.9 (6.0), 22.6 (15.0), and 56.6 (30.0) nm silica gel pores at a NaCl concentration of 3 wt % were measured and presented along with model calculations in Figure 5 and Table 3. In addition, three-phase H−$L_W$−V equilibria for the quaternary $CH_4$ (90%) + $C_3H_8$ (10%) + NaCl + water mixtures in 56.6 (30.0) nm silica gel pores at NaCl concentrations of 3 and 10 wt % were measured and presented along with model calculations in Figure 6 and Table 4. The combined effects of pores and electrolytes that closely simulate real marine sediments were investigated through checking the shift of the experimentally measured H−$L_W$−V curves. As can be seen in Figure 5, electrolytes themselves can inhibit gas hydrate formation. Also, within the pores, gas hydrates face a high pressure because of capillary effects, resulting in inhibition. In the solid-solution model, the stability conditions of hydrates are directly affected by the activity of water. As the activity decreases, the hydrates form at higher pressure at a specified temperature or at lower temperature at a specified pressure, which is called inhibition. The activity of water confined in the small pores is depressed by the partial ordering and bonding of water molecules with hydrophilic surfaces of pores.[20] The decrease in water activity due to the presence of geometrical constraints is considered to be equivalent to a change in its activity caused by electrolytes.[2] As can be seen in Figures 5 and 6, the H−$L_W$−V curves were shifted more to the inhibition region when compared to those in the either the bulk or pure state as the pore size decreases and electrolyte concentration increases. The activity of water in deep ocean sediment is affected by electrolytes dissolved in the seawater and is further affected by the capillary force due to the sediment pores. The combined effect

**Table 5. Calculated Lower Quadruple Points**

| system | pore size (nm) | $T$ (K) | $P$ (MPa) |
|---|---|---|---|
| $CH_4 + C_3H_8$ + water | 12.9 (6.0) | 267.2 | 0.353 |
| | 22.6 (15.0) | 269.7 | 0.399 |
| | 56.6 (30.0) | 271.5 | 0.43 |
| | 165.2 (100) | 272.2 | 0.441 |
| | bulk | 273.1 | 0.456 |
| $CH_4 + C_3H_8$ + NaCl | 12.9 (6.0) | 265.5 | 0.331 |
| (3 wt %) + water | 22.6 (15.0) | 267.9 | 0.37 |
| | 56.6 (30.0) | 269.7 | 0.398 |
| | bulk | 270.9 | 0.419 |
| system | NaCl (wt%) | $T$ (K) | $P$ (MPa) |
| $CH_4 + C_3H_8$ + NaCl + | 0 | 271.5 | 0.43 |
| Water in 56.6 (30.0) nm | 3 | 269.7 | 0.398 |
| | 10 | 264.6 | 0.319 |

of pores and electrolytes can remarkably shift the equilibrium condition to the inhibition region.

Although the experimental determinations of the ternary $CH_4$ (90%) + $C_3H_8$ (10%) + water mixtures and the quaternary $CH_4$ (90%)+ $C_3H_8$ (10%) + NaCl + water mixtures in silica gel pores were restricted to the H−$L_W$−V phase boundary because of some experimental difficulties in measuring the hydrate (H)−ice (I)−vapor (V) phase boundary, the model calculation could be extended to the three-phase boundary of H−I−V in Figures 4−6. As expected, the melting point of ice is depressed by the presence of geometrical constraints and electrolytes. The lower quadruple point ($Q_1$) where four phases (H, I, $L_W$, and V) coexist normally appears adjacent to the corresponding melting point of ice and is known to be a function of pore diameter and electrolyte concentration. In the present study, the lower quadruple temperature ($T_{Q_1}$) was determined as the intersection point of two calculated H−$L_W$−V and H−I−V phase boundaries. The values of $T_{Q_1}$ in the ternary $CH_4$ (90%) + $C_3H_8$ (10%) + water mixtures and the quaternary $CH_4$ (90%) + $C_3H_8$ (10%) + NaCl + water mixtures in silica gel pores decreased from those of the corresponding bulk or pure states as the pore size decreased and the NaCl concentration increased. However, it should be noted that the H−I−V equilibrium line was not dependent on pore size and electrolyte concentration because the interfacial tension between ice and hydrate phases ($\sigma_{IH}$) was assumed to be zero in this study. The calculated $Q_1$ values for the ternary $CH_4$ (90%) + $C_3H_8$ (10%) + water mixtures and the quaternary $CH_4$ (90%) + $C_3H_8$ (10%) + NaCl + water mixtures in the bulk state and silica gel pores were listed in Table 5. Although the present pore hydrate model accounting for the capillary effect and electrolyte inhibition was proven to be quite reliable both qualitatively and quantitatively, the percent average absolute deviations (%AADs) between experimental and calculated H−$L_W$−V values are listed in Table 6 for reference. The predicted H−$L_W$−V values were generally in good agreement with the experimental ones.

In the present study, NMR spectroscopy was adopted to analyze the solid hydrate phase of the mixed-gas hydrate because NMR spectroscopy has been recognized as a powerful tool for the identification of gas hydrate structures and compositions.[22] In particular, cage-dependent $^{13}C$ NMR chemical shifts for the enclathrated guest molecules can be used to determine structure types of the formed gas hydrates. Figure 7 shows a stacked plot of the $^{13}C$ MAS NMR spectra of pure $CH_4$, pure $C_3H_8$, and mixed $CH_4 + C_3H_8$ hydrates. The pure $CH_4$ hydrate (sI) spectrum has two peaks at −6.6 and −4.3 ppm, respectively. Considering that the ideal stoichiometric ratio of the small $5^{12}$ to the large $5^{12}6^2$

(22) Ripmeester, J. A.; Ratcliffe, C. I. *J. Struct. Chem.* **1999**, *40*, 654.

**Table 6. Percent AAD between the Experimental and Calculated Values**

| system | pore size (nm) | %AAD |
|---|---|---|
| $CH_4 + C_3H_8$ + water | 12.9 (6.0) | 5.9 |
| | 22.6 (15.0) | 4.6 |
| | 56.6 (30.0) | 1.1 |
| | 165.2 (100) | 2.1 |
| | bulk | 2.3 |
| $CH_4 + C_3H_8$ + NaCl | 12.9 (6.0) | 7.5 |
| (3 wt %) + water | 22.6 (15.0) | 8.8 |
| | 56.6 (30.0) | 2.6 |
| | bulk | 7.1 |
| system | NaCl (wt %) | %AAD |
| $CH_4 + C_3H_8$ + NaCl + | pure | 1.1 |
| water in 56.6 (30.0) nm | 3 | 2.6 |
| | 10 | 3.7 |

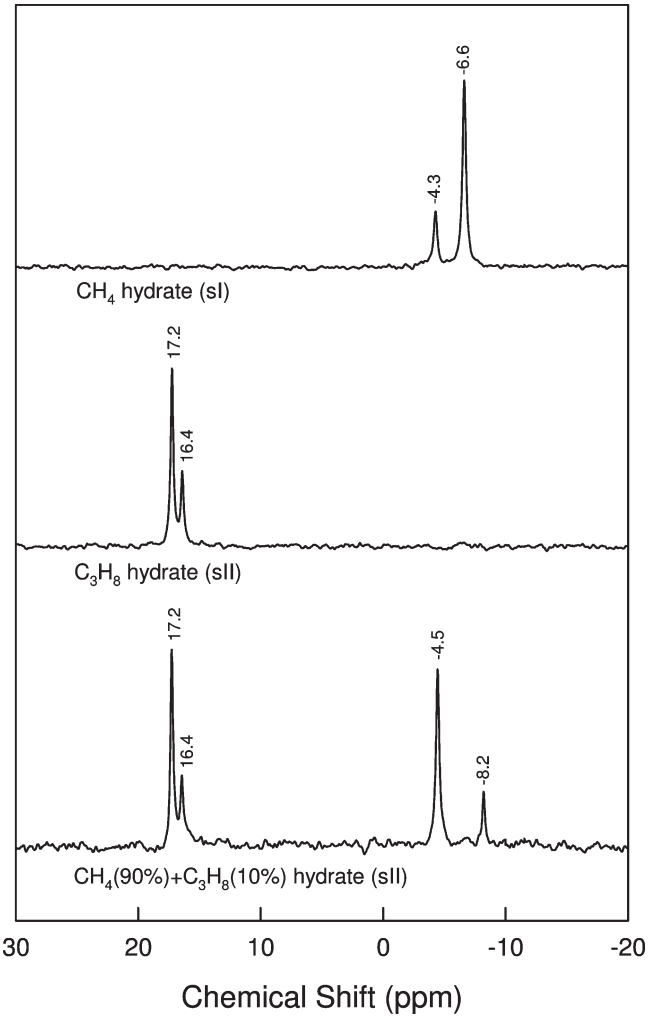


**Figure 7.** $^{13}C$ NMR spectra of the pure $CH_4$, pure $C_3H_8$, and mixed $CH_4$ (90%) + $C_3H_8$ (10%) gas hydrates.

cages in the unit cell of sI is 1:3, the peak at −4.3 ppm can be assigned to $CH_4$ molecules in the small $5^{12}$ cages and the peak at −6.6 ppm can be assigned to $CH_4$ molecules in the large $5^{12}6^2$ cage. However, for the pure $C_3H_8$ hydrate that is known to form sII, $C_3H_8$ molecules trapped only in the large sII $5^{12}6^4$ cages because of the size limitation were identified by two distinct resonance lines, one from $-CH_2-$ (at 16.4 ppm) and the other from $CH_3-$ (at 17.2 ppm). For the mixed $CH_4 + C_3H_8$ hydrate,

the $^{13}C$ MAS NMR spectrum indicates that the positions of two distinct resonance lines from captured $C_3H_8$ molecules are the same as those in the pure $C_3H_8$ hydrate; accordingly, the mixed $CH_4 + C_3H_8$ hydrate is confirmed to be sII. Only a very slight difference between chemical shifts of two $CH_4$ peaks representing the small $5^{12}$ cages of sI and sII was observed because both small cages of sI and sII consist of the pentagonal dodecahedra ($5^{12}$) of nearly the same dimension. On the contrary, the chemical shifts of $CH_4$ molecules in the large $5^{12}6^2$ (−6.6 ppm) and $5^{12}6^4$ (−8.2 ppm) cages of sI and sII showed distinct discrepancy for the enclathrated $CH_4$ molecules because the size and shape of each large cage are quite different. Accordingly, the $CH_4$ chemical shift pattern of large sI and sII cages can be used as a clear indicator to determine the structure types of the formed gas hydrates. The NMR chemical shifts of the present study for enclathrated $CH_4$ and $C_3H_8$ molecules are identical to those in the literature reports.[7,23,24]

To determine the occupancies of $CH_4$ and $C_3H_8$ molecules in the small and large cages of the gas hydrate structure, the relative integrated intensities of $^{13}C$ MAS NMR spectra must be combined with the following statistical thermodynamic expression representing the chemical potential of water molecules in sI and sII. In the absence of guest−guest interactions and host−lattice distortions, the chemical potentials of water molecules of sI and sII are, respectively, given by[14]

$$\mu_W(h) - \mu_W(h^0) = \frac{RT}{23}[3\ln(1-\theta_{l,CH_4}) + \ln(1-\theta_{s,CH_4})] \quad (12)$$

$$\mu_W(h) - \mu_W(h^0) = \frac{RT}{17}[\ln(1-\theta_{l,C_3H_8} - \theta_{l,CH_4}) + 2\ln(1-\theta_{s,CH_4})] \quad (13)$$

where $\mu_W(h°)$ is the chemical potential of water molecules of a hypothetical empty lattice and $\theta_S$ and $\theta_l$ are the fractional occupancies of small and large cages, respectively. When the gas hydrate is in equilibrium with ice, the left side of the above equation becomes $\mu_W(\text{ice}) - \mu_W(h°) = -\Delta\mu_W^\circ$ where $\Delta\mu_W^\circ$ is the chemical potential of the empty lattice relative to ice. The values of $\Delta\mu_W^\circ$ used in this work are 1297 J/mol for sI and 883.8 J/mol for sII.[1] After integrating each peak in the spectra and considering the facts that there are three times as many large $5^{12}6^2$ cages as small $5^{12}$ ones in sI and two times as many small $5^{12}$ cages as large $5^{12}6^4$ ones in sII, the actual values of cage occupancy ratios were substituted into the above equations to calculate the cage occupancies of each molecule, and the resulting values are listed in Table 7. From the $^{13}C$ NMR spectral results, it can be concluded that the mixed $CH_4$ (90%) + $C_3H_8$ (10%) gas hydrate is sII and the small cages are occupied by $CH_4$ molecules whereas the large cages are shared by $CH_4$ and $C_3H_8$ molecules.

**Table 7. Cage Occupancies of the Pure $CH_4$ and Mixed $CH_4 + C_3H_8$ Hydrates**

| | | $CH_4$ | | $C_3H_8$ |
|---|---|---|---|---|
| system | structure | $\theta_{s,CH_4}$ | $\theta_{l,CH_4}$ | $\theta_{l,C_3H_8}$ |
| $CH_4$ + water | sI | 0.894 | 0.974 | |
| $CH_4 + C_3H_8$ + water | sII | 0.732 | 0.352 | 0.630 |

## Conclusions

Three-phase H−$L_W$−V equilibria for the ternary $CH_4$ (90%) + $C_3H_8$ (10%) + water mixtures in silica gel pores with nominal diameters of 6.0, 15.0, 30.0, and 100.0 nm and for the quaternary $CH_4$ (90%) + $C_3H_8$ (10%) + NaCl + water mixtures of two different NaCl concentrations (3 and 10 wt %) in silica gel pores with nominal diameters of 6.0, 15.0, and 30.0 nm were measured and compared with the calculated results based on the van der Waals and Platteeuw model. A correction term for the capillary effect and a Pitzer model for electrolyte solutions were adopted to calculate the activity of water in the aqueous electrolyte solutions within silica gel pores. A $CH_4$ (90%) + $C_3H_8$ (10%) hydrate−water interfacial tension ($\sigma_{HW}$) of 42 ± 3 mJ/m$^2$ was obtained through the Gibbs−Thomson equation for dissociation within the cylindrical pores, and with this value, the calculated results of H−$L_W$−V equilibria were in good agreement with the experimental ones. The combined inhibition effects of pores and electrolytes were observed in the experimental and calculated values of the three-phase H−$L_W$−V equilibria. It was confirmed that the structure of the mixed $CH_4$ (90%) + $C_3H_8$ (10%) gas hydrate is sII and that large cages of sII are shared by $CH_4$ and $C_3H_8$ hydrates whereas small cages are occupied only by $CH_4$ molecules. The overall thermodynamic and spectroscopic results obtained from this study can be used to understand the fundamental phase behavior and structural details of the mixed-gas hydrates in silica gel pores filled with electrolyte solution and thus could be applied as valuable key information in developing the natural gas hydrate in marine sediments.

**Acknowledgment.** This work is the outcome of a Manpower Development Program for Energy & Resources supported by the Ministry of Knowledge Economy (MKE) and was also supported by the Basic Science Research Program through the National Research Foundation of Korea (NRF) funded by the Ministry of Education, Science and Technology (2009-0069569). We also acknowledge funding from the Korea Ministry of Knowledge Economy (MKE) through the "Energy Technology Innovation Program". We thank Mrs. S. H. Kim and Dr. O. H. Han (KBSI) for their support with respect to NMR measurements.

(23) Kim, D. Y.; Lee, J.-w.; Seo, Y. T.; Ripmeester, J. A.; Lee, H. *Angew. Chem., Int. Ed.* **2005**, *44*, 7749.
(24) Seo, Y.; Kang, S. P.; Jang, W. *J. Phys. Chem. A* **2009**, *113*, 9641.
(25) Deaton, W. M.; Frost, E. M., Jr. *U.S. Bur. Mines, Monogr.* **1946**, *8*, 101.